Effects of SnxPty Alloy Structures on the Performance of SnPt Catalysts for the Selective Hydrogenation of Unsaturated Aldehydes to Unsaturated Alcohols

Taniya, Keita
Ichihashi, Yuichi
Nishiyama, Satoru

(Citation)
Journal of the Japan Petroleum Institute,63(2):52-61

(Issue Date)
2020-03-01

(Resource Type)
journal article

(Version)
Version of Record

(URL)
https://hdl.handle.net/20.500.14094/90007630

[Review Paper]

Effects of Sn_xPt_y Alloy Structures on the Performance of SnPt Catalysts for the Selective Hydrogenation of Unsaturated Aldehydes to Unsaturated Alcohols

Keita TANIYA*, Yuichi ICHIHASHI, and Satoru NISHIYAMA

Dept. of Chemical Science and Engineering, Graduate School of Engineering, Kobe University, 1-1 Rokkodai, Nada-ku, Kobe 657-8501, JAPAN

(Received September 17, 2019)

The development of next-generation heterogeneous catalysts for the chemoselective hydrogenation of unsaturated aldehydes to unsaturated alcohols requires extensive structural understanding of active catalyst sites. In the case of SnPt catalysts, the presence of metallic Sn and the formation of Sn–Pt alloys are believed to be key factors strongly affecting the selectivity of unsaturated alcohol formation. This review describes the relationship between the catalytic crotonaldehyde (CH_3–CH = CH–CHO) hydrogenation performance of supported and non-supported SnPt catalysts and the structure of the component Sn_xPt_y alloys, which reveal that at the same Sn/Pt atomic ratio, the composition of the produced Sn_xPt_y alloys depends on the preparation method. The Sn_1Pt_3, Sn_1Pt_1, and Sn_2Pt_1 phases identified in SnPt catalysts exhibited higher crotyl alcohol (CH_3–CH = CH–CH_2OH) formation selectivity than the monometallic Pt phase. Furthermore, the Sn_1Pt_1 and Sn_2Pt_1 phases showed lower crotonaldehyde conversion than the Pt phase. Formation of Sn oxides over the supported SnPt catalysts was confirmed with excess amount of Sn. The crotyl alcohol selectivity increased with the transition from Sn_1Pt_3 to Sn_1Pt_1, then decrease with the further transition to the more Sn-rich Sn_2Pt_1 phase. Thus, the Sn_1Pt_1 alloy phase was concluded to be the most effective bimetallic SnPt structure for the selective formation of crotyl alcohol.

Keywords

Selective hydrogenation, Tin platinum catalyst, Nanoparticle, Unsaturated aldehyde, Unsaturated alcohol

1. Introduction

Chemoselective reactions convert specific functional groups of a multifunctional compound into other moieties, so are extremely important for the synthesis of value-added chemicals, such as the selective hydrogenation of unsaturated aldehydes to the corresponding unsaturated alcohols, which are used for perfume, pharmaceutical, and fine chemical production[1)~4)].

The formation of saturated aldehydes preferentially proceeds over conventional (*e.g.*, supported group VIII metal) hydrogenation catalysts. The modification of noble metal catalysts with secondary metals or their oxides is reported to prevent C = C bond hydrogenation and/or promote C = O bond hydrogenation to improve the selectivity for unsaturated alcohol formation[1)~4)]. **Scheme 1** shows the reaction pathway for the hydrogenation of crotonaldehyde as a model unsaturated aldehyde to form crotyl alcohol (UOL) or butyraldehyde (SAL), both of which can be further hydrogenated to generate 1-butanol (SOL).

Bimetallic SnPt catalysts are widely used for the hydrogenation of unsaturated aldehydes[5)~22)]. The catalytic performance of supported SnPt catalysts depends on factors such as the Sn/Pt atomic ratio[7)~12)], types of precursors and supports[12)~16)], and preparation procedures/conditions[9)~12),15)~22)]. The function of the Sn component is not yet fully understood, but the improvement in catalytic selectivity achieved by inclusion of Sn has been ascribed to two effects. First, ionic Sn species (Sn^{2+} or Sn^{4+}) are believed to interact with the carbonyl oxygen of unsaturated aldehydes, resulting in activation of the C = O group and acceleration of the hydrogenation reaction[7),11),13),14),17),19),21)]. Second, metallic Sn is thought to dilute the Pt ensembles and form Sn–Pt alloys[7),13)~15),17),20),22)]. Pt ensembles are known to activate the C = C bonds of unsaturated aldehydes, thus catalyzing the undesired formation of saturated compounds, so dilution of Pt ensembles prevents C = C bond hydrogenation in unsaturated aldehydes and alcohols.

The well-characterized Sn–Pt phase diagram describes the formation of five different alloy phases, face-centered cubic (fcc) Sn_1Pt_3, hexagonal Sn_1Pt_1, hex-

DOI: doi.org/10.1627/jpi.63.52

* To whom correspondence should be addressed.
* E-mail: taniya@platinum.kobe-u.ac.jp

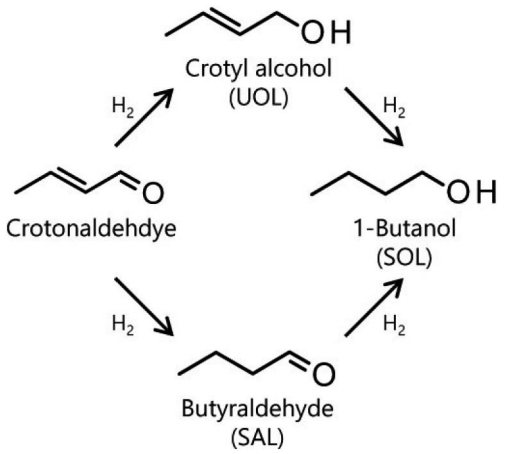

Scheme 1 Crotonaldehyde Hydrogenation Pathway

agonal Sn_3Pt_2, cubic Sn_2Pt_1, and orthorhombic Sn_4Pt_1[23]. However, the relationships between the properties of Sn_xPt_y alloys and their catalytic activities are not yet understood, as mono- and bimetallic phases cannot be observed in the very active SnPt bimetallic catalysts because of the presence of highly dispersed metal species[11]. Therefore, investigation of the catalytic behavior of specific Sn_xPt_y alloys for unsaturated aldehyde hydrogenation may facilitate the design of SnPt catalysts with high selectivity for unsaturated alcohols.

The present study describes the hydrogenation of crotonaldehyde over SiO_2-supported SnPt catalysts prepared by co-impregnation[24] and successive impregnation[25], and over SnPt nanoparticles (SnPt-NPs) synthesized by a polyalcohol reduction method[24]. The bulk structures of SnPt catalysts were analyzed by X-ray diffraction (XRD) to identify the most effective SnPt structure and composition. Furthermore, the relationships between Sn_xPt_y alloy structures and their catalytic performance for the hydrogenation of crotonaldehyde to UOL are discussed.

2. Effect of Preparation Method and Sn/Pt Atomic Ratio on Crotonaldehyde-to-crotyl-alcohol Hydrogenation Activity of Supported SnPt Catalysts

2. 1. Preparation of SiO_2-supported SnPt Catalysts by Different Impregnation Methods

2. 1. 1. Preparation by Co-impregnation (Sn−Pt/SiO_2)

Silica Q-10 (Fuji Silysia Chemical Ltd.), used as a support to prepare SnPt catalysts, was calcined in a flow of air at 773 K for 5 h and then co-impregnated with an ethanolic solution of $H_2PtCl_6 \cdot 6H_2O$ (Tanaka Kikinzoku Kogyo Co.) and $SnCl_2 \cdot 2H_2O$ (Nacalai Tesque, Inc.) at 353 K. The obtained samples were dried overnight at 393 K, calcined in a flow of air at 823 K for 2 h, and reduced in a flow of H_2 at 573 K for 2 h to afford Sn-Pt/SiO_2 catalysts with a Pt loading on SiO_2 of 4 wt% and Sn/Pt atomic ratios of 0.2-2.0.

2. 1. 2. Preparation by Successive Impregnation (Sn/Pt/SiO_2)

Silica Q-10, used as the support for preparing Sn/Pt/SiO_2 catalysts, was pretreated in the same way as SiO_2 during the preparation of co-impregnated Sn-Pt/SiO_2 catalysts (section **2. 1. 1.**). SiO_2-supported Pt catalyst (Pt/SiO_2) was prepared by impregnating SiO_2 with an aqueous solution of $H_2PtCl_6 \cdot 6H_2O$ (Tanaka Kikinzoku Kogyo Co.) diluted with ethanol at 353 K. The impregnated sample was dried overnight at 393 K, calcined in a flow of air at 823 K for 2 h, and reduced in a flow of H_2 at 573 K for 2 h. The loading of Pt on the SiO_2 support was 4 wt%. Bimetallic Sn/Pt/SiO_2 catalysts were prepared from Pt/SiO_2 as described above, except that the H_2 reduction step was omitted, then the Pt/SiO_2 sample was impregnated with an ethanolic solution of $SnCl_2 \cdot 2H_2O$ (Nacalai Tesque, Inc.) at 353 K followed by overnight drying at 393 K, calcination for 2 h in a flow of air at 823 K, and reduction for 2 h in a flow of H_2 at 573 K. The Sn/Pt atomic ratio varied from 0.2 to 2.0.

2. 2. Chemoselective Hydrogenation of Crotonaldehyde over SiO_2-supported SnPt Catalysts

The effect of the Sn/Pt atomic ratio on the performance of Sn/Pt/SiO_2 and Sn-Pt/SiO_2 catalysts was assessed by performing liquid-phase hydrogenation of crotonaldehyde (0.2 mL) in 2-methyl-2-butanol (4.0 mL) in a stainless-steel autoclave (30 mL) at 373 K under H_2 at 2.0 MPa (gauge). The catalyst weight/reaction time was 25 mg/1 h and 50 mg/20 h for Sn-Pt/SiO_2 and Sn/Pt/SiO_2, respectively.

2. 2. 1. Effect of Sn/Pt Atomic Ratio on the Performance of Sn-Pt/SiO_2 Catalysts Prepared by Co-impregnation

Figure 1 shows the conversion and selectivity for crotonaldehyde hydrogenation over co-impregnation-prepared Sn-Pt/SiO_2 catalysts. Crotonaldehyde conversion gradually decreased with higher Sn/Pt atomic ratio (**Fig. 1(a)**), whereas SOL selectivity was maintained at ～15 % irrespective of this ratio, and UOL selectivity increased with higher Sn/Pt atomic ratio (**Fig. 1(b)**). The highest UOL selectivity of ～50 % was observed at ～3 % conversion and Sn/Pt = 2.0.

The presence of mono- and bimetallic structures containing Sn and/or Pt was investigated by XRD, which revealed peaks attributable to reduced Pt metal[26),27] (2θ = 39.5° and 46.5°), Sn_1Pt_3[28] (2θ = 38.8° and 48.6°), Sn_1Pt_1[29),30] (2θ = 25.0 30.0, 41.5, and 44.0°), and Sn_2Pt_1[15] (2θ = 24.0, 40.0, 47.0, and 57.5°).

Figure 2 presents the XRD patterns of co-impregnation-synthesized Sn-Pt/SiO_2 catalysts, showing that the characteristic peaks of fcc crystalline Pt were observed for Pt/SiO_2 (Sn/Pt = 0) (**Fig. 2** (a)) and Sn-Pt/SiO_2 (Sn/Pt = 0.2 and 0.5) (**Figs. 2** (b) and (c), respectively).

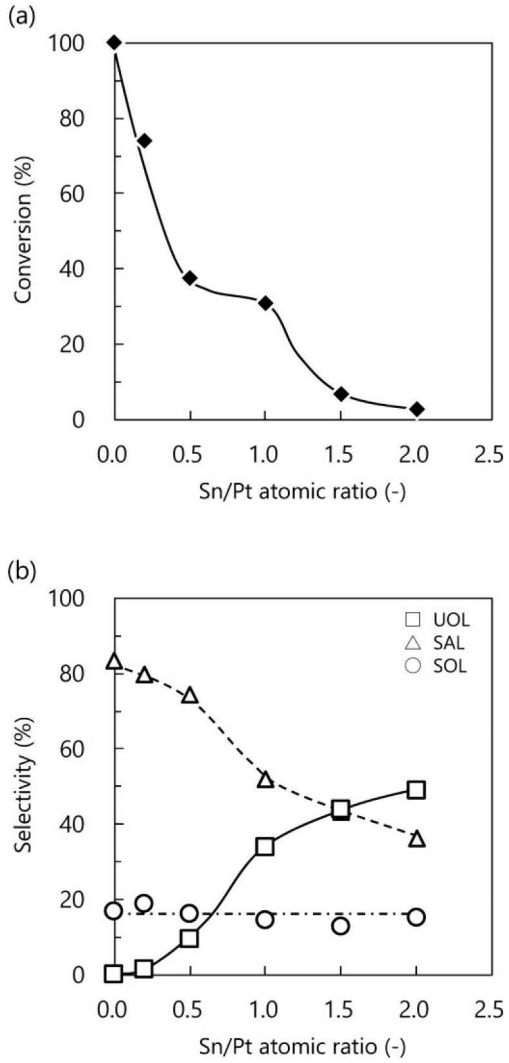

Fig. 1 Effect of the Sn/Pt Atomic Ratio of Sn–Pt/SiO_2 Catalysts Prepared by Co-impregnation on (a) Conversion and (b) Product Formation Selectivity during Crotonaldehyde Hydrogenation[24)]

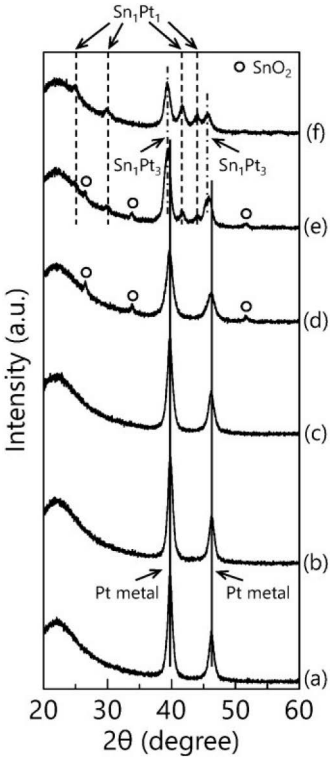

The diffraction patterns were recorded at a scanning speed of 0.5°/min.

Fig. 2 XRD Patterns of Sn–Pt/SiO_2 Catalysts Prepared by Co-impregnation with Sn/Pt = 0 (a), 0.2 (b), 0.5 (c), 1.0 (d), 1.5 (e), and 2.0 (f)[24)]

For the catalyst with Sn/Pt = 1 (**Fig. 2** (d)), the peaks of reduced Pt metal were shifted to slightly lower angles. As the Sn_1Pt_3 peaks appeared close to the reduced Pt metal peaks, this peak shift was ascribed to the formation of small amounts of Sn_1Pt_3 and the resulting overlap of its peaks with those of reduced Pt metal. Additionally, Sn_1Pt_1 was observed at Sn/Pt = 1.5-2.0 (**Figs. 2** (e) and (f)), and the peak intensities of Sn_1Pt_3 and Sn_1Pt_1 decreased and increased, respectively, with higher Sn content. For Sn/Pt = 1.0-2.0 (**Figs. 2** (d)-(f)), the peaks of SnO_2 appeared at $2\theta = 27.0$, 34.0, and 52.0°, which suggested that some Sn species did not interact with Pt species in Sn–Pt/SiO_2 catalysts.

Formation of Sn_1Pt_3 and Sn_1Pt_1 alloys over Sn–Pt/SiO_2 catalysts decreased the conversion (**Fig. 1(a)**) and SAL selectivity (**Fig. 1(b)**) but increased UOL selectivity (**Fig. 1(b)**), which suggested that Sn_xPt_y alloy generation affects the catalytic selectivity for unsaturated aldehyde hydrogenation.

2. 2. 2. Effect of Sn/Pt Atomic Ratio on Catalytic Performance of Sn/Pt/SiO_2 Catalysts Prepared by Successive Impregnation

Figure 3 shows the catalytic activity and selectivity for crotonaldehyde hydrogenation over Sn/Pt/SiO_2 catalysts prepared by successive impregnation. At Sn/Pt = 0, the main product was SAL and no UOL was formed (**Fig. 3(b)**). At $0 < Sn/Pt \leq 1.0$, crotonaldehyde conversion was maintained at 100 %, but significantly decreased at higher Sn/Pt ratios (**Fig. 3(a)**). UOL selectivity (**Fig. 3(b)**) increased with higher Sn/Pt ratios up to 0.5 and was maintained at ～70 % at $0.5 \leq Sn/Pt \leq 1.0$, increasing to ～90 % at Sn/Pt = 1.2-2.0. Therefore, Sn/Pt/SiO_2 catalysts prepared by successive impregnation provided better UOL selectivity than Sn–Pt/SiO_2 catalysts prepared by co-impregnation.

Figure 4 shows the XRD patterns of Sn/Pt/SiO_2 catalysts prepared by successive impregnation, revealing that Pt metal peaks were shifted to slightly lower angles at Sn/Pt = 0.2 (**Fig. 4** (b)) and demonstrating the coexistence of Sn_1Pt_3 and Sn_1Pt_1 at Sn/Pt = 0.5 (**Fig. 4** (c)). At Sn/Pt > 0.5, the intensities of the Sn_1Pt_3 peaks decreased with higher Sn content (**Figs. 4** (c)-(g)),

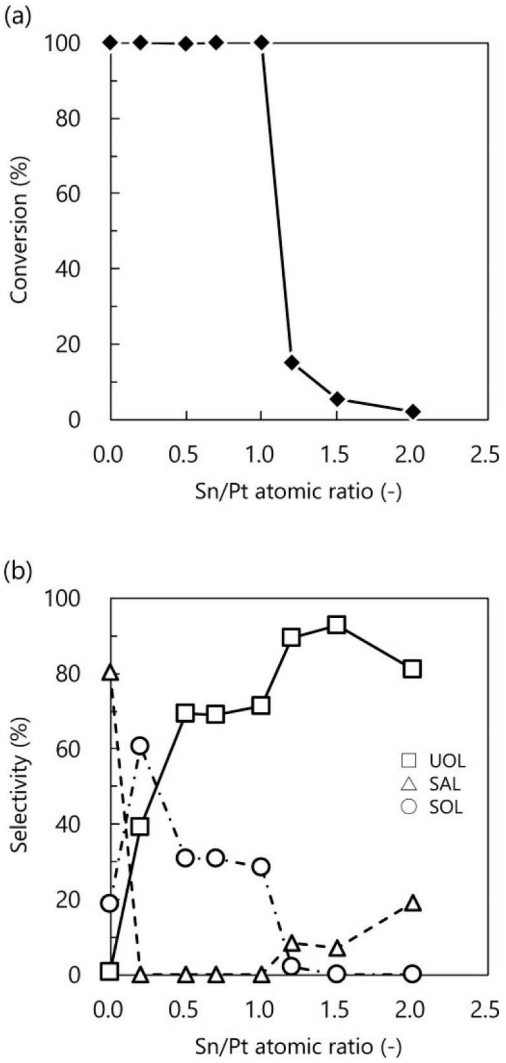

Fig. 3 Effect of the Sn/Pt Atomic Ratio of $Sn/Pt/SiO_2$ Catalysts Prepared by Successive Impregnation on (a) Conversion and (b) Product Formation Selectivity during Crotonaldehyde Hydrogenation[25)]

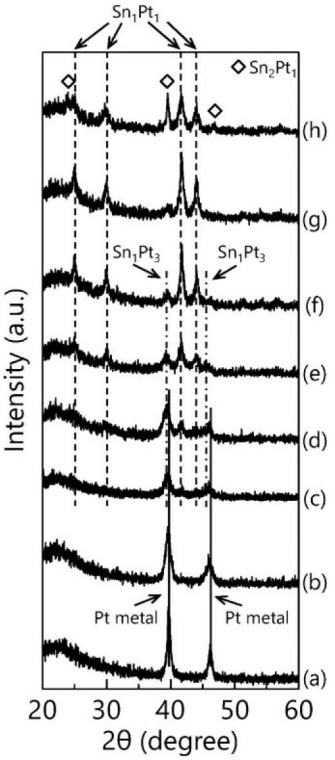

The diffraction patterns were recorded at a scanning speed of 4.0°/min.

Fig. 4 XRD Patterns of $Sn/Pt/SiO_2$ Catalysts Prepared by Successive Impregnation with Sn/Pt = 0 (a), 0.2 (b), 0.5 (c), 0.7 (d), 1.0 (e), 1.2 (f), 1.5 (g), and 2.0 (h)[25)]

whereas the intensity of the Sn_1Pt_1 peaks increased up to Sn/Pt = 1.5 (**Figs. 2** (c)-(g)), decreasing with higher Sn content at higher Sn/Pt ratios (**Fig. 2** (h)). At Sn/Pt = 2.0 (**Fig. 2** (h)), Sn_2Pt_1 peaks appeared.

Although the supported SnPt catalysts were prepared at the same Sn/Pt atomic ratios, their phase composition depended on the impregnation method. For instance, at Sn/Pt = 1.0, Pt metal, Sn_1Pt_3, and SnO_2 were formed in Sn–Pt/SiO_2 catalysts (**Fig. 2** (d)), whereas Sn_1Pt_3 and Sn_1Pt_1 were formed in $Sn/Pt/SiO_2$ catalysts (**Fig. 4** (e)). In addition, the composition of the Sn_xPt_y alloy structures formed in $Sn/Pt/SiO_2$ catalysts prepared by successive impregnation was close to that expected from the bulk Sn/Pt atomic ratios, whereas that of Sn–Pt/SiO_2 catalysts prepared by co-impregnation was lower than expected. Thus, Sn and Pt species were presumably better mixed in the former case. Further investigation is required to clarify why the preparation methods affect the state of mixing of Sn and Pt.

Sn_1Pt_1 formation apparently increased UOL formation selectivity in $Sn/Pt/SiO_2$ catalysts. The UOL and SOL selectivities (**Fig. 3(b)**) were almost constant and independent of the Sn/Pt ratio at $0.5 \leq Sn/Pt \leq 1.0$, although the intensities of the Sn_1Pt_3 and Sn_1Pt_1 peaks decreased and increased, respectively (**Figs. 4** (c)-(e)), with higher Sn content. Assuming that the surface area occupied by these alloys varied, the UOL and SOL selectivities were expected to increase and decrease, respectively, with higher Sn/Pt atomic ratio because of the concomitant dilution of Pt ensembles by Sn. Consequently, the formation of Sn_1Pt_1 presumably proceeded from the surface to the inside of Sn- and Pt-containing particles, so that the surface area occupied by Sn_1Pt_1 remained constant at Sn/Pt = 0.5-1.0.

Figure 5 displays the Sn/Pt-ratio-dependent H_2 and CO chemisorption capacities of $Sn/Pt/SiO_2$ catalysts prepared by successive impregnation, revealing that the addition of a small amount of Sn to Pt/SiO_2 (Sn/Pt = 0.2) sharply inhibited irreversible H_2 and CO adsorption. At $Sn/Pt \geq 0.2$, the CO chemisorption capacity exceeded the H_2 chemisorption capacity, presumably because dissociative H_2 adsorption requires at least two

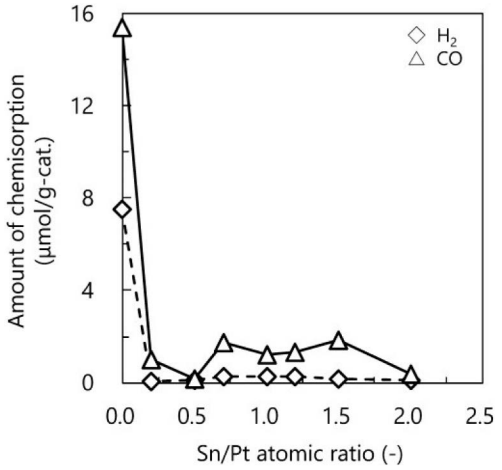

Fig. 5 Effect of the Sn/Pt Atomic Ratio on H_2 and CO Adsorption Capacities of Sn/Pt/SiO_2 Catalysts Prepared by Successive Impregnation

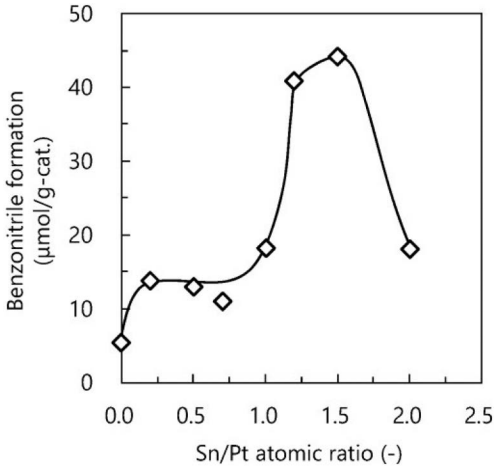

Fig. 6 Effect of the Sn/Pt Atomic Ratio on Benzonitrile Formation over Sn/Pt/SiO_2 Catalysts Prepared by Successive Impregnation, as Evaluated by Benzaldehyde–Ammonia Titration (BAT)

adjacent Pt atoms, whereas effective CO adsorption requires only one vacant Pt atom. Additionally, H_2 and CO cannot be chemisorbed on metallic Sn. These results indicate that successively impregnated Sn species can easily interact with Pt to form Sn_xPt_y alloys and thus dilute Pt ensembles, consistent with the well-known ensemble effect of bimetallic catalysts[31].

The amount of surface Sn oxides present in Sn/Pt/SiO_2 catalysts was evaluated by benzaldehyde–ammonia titration (BAT), which can determine the surface amount of basic metal cations using a pulse technique[32)~36)]. First, benzaldehyde is adsorbed until saturation on the basic sites of the metal oxide surface to form benzoate anions, which react with ammonia (supplied in pulses) to form easily desorbed benzonitrile. The amount of produced benzonitrile indicates the amount of surface metal oxides.

Figure 6 shows the effect of the Sn/Pt ratio of Sn/Pt/SiO_2 catalysts on the amount of benzonitrile (*i.e.*, the amount of surface Sn oxides) formed during BAT. For Pt/SiO_2, benzonitrile production reached 5.5 μmol/g-cat., which suggested that benzaldehyde can be adsorbed on the SiO_2 surface[34]. The addition of a small amount of Sn (Sn/Pt = 0.2) facilitated benzonitrile formation, and benzonitrile productivity was maintained at Sn/Pt = 0.2-1.0. These results imply that fine Sn oxide particles undetectable by XRD were formed on the Sn/Pt/SiO_2 catalysts. Significantly higher amounts of benzonitrile were formed at Sn/Pt = 1.2-1.5 (**Fig. 6**). As shown in **Figs. 3** and **6**, the conversion of crotonaldehyde considerably decreased at Sn/Pt = 1.2 (**Fig. 3(a)**), presumably because of the concomitant increase in the amount of Sn oxides (**Fig. 6**). These oxides were presumably located on the surface of Sn_1Pt_1 alloy particles and suppressed H_2 activation. Further addition of Sn considerably inhibited benzonitrile formation, presumably due to the sintering of Sn species and/or Sn_2Pt_1 formation (**Fig. 4** (h)).

Scheme 2 presents the mechanism of crotonaldehyde hydrogenation over Sn/Pt/SiO_2 catalysts with different Sn/Pt atomic ratios prepared by successive impregnation. In the case of Pt/SiO_2 (Sn/Pt = 0), C = C bond activation over the Pt surface leads to the preferential formation of SAL (**Scheme 2(a)**). Introduction of Sn into Pt/SiO_2 promoted both UOL and SOL formation (**Fig. 3(b)**), and no SAL formation was observed at Sn/Pt = 0.2-1.0, which indicated preferential crotonaldehyde and SAL C = O bond hydrogenation. At Sn/Pt = 0.5-1.0, the UOL and SOL selectivities were maintained (**Fig. 3(b)**) despite the concomitant increase of Sn content during the transition from Sn_1Pt_3 to Sn_1Pt_1 (**Figs. 4** (c)-(e)). These results suggest that a core-shell structure comprising a Sn_1Pt_3 core and a Sn_1Pt_1 shell is presumably formed in the bimetallic active sites, and the growth of the Sn_1Pt_1 shell with higher Sn/Pt ratio results in a constant surface composition (**Scheme 2(b)**). At Sn/Pt ≥ 1.2, hydrogenation activity significantly decreased (**Fig. 3(a)**), presumably due to the suppression of hydrogen activation with the facilitated formation of Sn oxides over SnPt bimetallic active sites, as indicated by the BAT measurements (**Fig. 6**). In this Sn/Pt ratio range, Pt ensembles are further diluted by the formation of Sn_2Pt_1 and/or covered with Sn oxides, which further enhances UOL selectivity (**Scheme 2(c)**).

In the case of SiO_2-supported SnPt catalysts, the impregnation method affected the formation of Sn_xPt_y at the same Sn/Pt atomic ratio, resulting in different catalytic performance for selective crotonaldehyde hydrogenation. The co-existence of Sn_1Pt_3 and Sn_1Pt_1, and that of Sn_1Pt_1 and SnO_2, seems to be responsible for the selective formation of UOL.

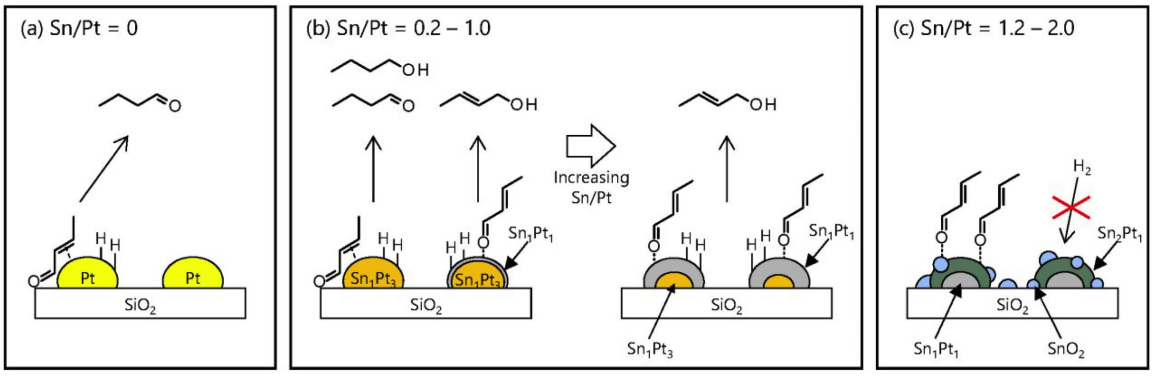

Scheme 2 Suggested Mechanism of Crotonaldehyde Hydrogenation over Sn/Pt/SiO_2 Catalysts Prepared by Successive Impregnation with Sn/Pt = (a) 0, (b) 0.2-1.0, and (c) 1.2-2.0

3. Effect of Sn/Pt Atomic Ratio on Crotonaldehyde-to-crotyl-alcohol Hydrogenation over SnPt–NP Catalysts

As mentioned earlier, several Sn sites including Sn_xPt_y and Sn oxides are concurrently formed over SiO_2-supported SnPt catalysts prepared by co-impregnation and successive impregnation, resulting from the strong metal-support interactions. The presence of various Sn sites on SnPt catalysts makes it difficult to elucidate the specific sites responsible for the selective formation of unsaturated alcohols. To exclude the metal-support interaction during catalyst preparation, unsupported SnPt–NP catalysts were prepared using a polyalcohol reduction method[24].

3. 1. Preparation of SnPt–NP Catalysts

SnPt–NP catalysts were prepared by a polyalcohol reduction method described elsewhere[37)~39)]. A 50 mL three-neck round-bottom flask was charged with 0.197 g of platinum(II) acetylacetonate ($Pt(acac)_2$, Tanaka Kikinzoku Kogyo Co.), 0-0.12 g of tin(II) acetate ($Sn(OAc)_2$, Aldrich), 0.34 mL of oleylamine (Aldrich), 0.32 mL of oleic acid (Nacalai Tesque, Inc.), 0.78 g of 1,2-hexadecanediol (Tokyo Chemical Industry Co., Ltd.), and 20 mL of dioctyl ether (Tokyo Chemical Industry Co., Ltd.). The amount of $Sn(OAc)_2$ was varied to control the Sn/Pt ratio. The Sn/Pt atomic ratio in the starting mixture for polyalcohol reduction was 0, 0.2, 0.5, 0.7, 1.0, 1.2, or 1.5 of the catalyst. The mixture was bubbled with N_2, heated to 533 K using a heating mantle, maintained under reflux for 1 h, cooled to room temperature, diluted with ethanol (Nacalai Tesque, Inc.), and centrifuged to separate the nanoparticles. The precipitate was rinsed three times with ethanol and dried *in vacuo* at room temperature to obtain the SnPt–NP catalysts, and the Sn/Pt ratios were determined by atomic adsorption spectroscopy.

3. 2. Structural Properties of SnPt–NP Catalysts

The morphologies of Pt–NP (Sn/Pt = 0) and SnPt–NP (Sn/Pt = 1.40) catalysts observed by transmission electron microscopy (TEM) are shown in **Fig. 7**. Pt–NP catalysts (**Fig. 7(a)**) consisted of polyhedral nanoparticles with diameters of 10-20 nm, whereas SnPt–NP catalysts with Sn/Pt = 1.40 (**Fig. 7(b)**) contained quasi-spherical nanoparticles with diameters of 2-10 nm. Both Pt–NP and SnPt–NP catalysts were synthesized under the same conditions except for the amount of Sn introduced during the polyalcohol reduction, but their nanoparticle sizes were different, probably because of the presence of a second metal. A similar effect of a second metal on nanoparticle size has been reported previously[39].

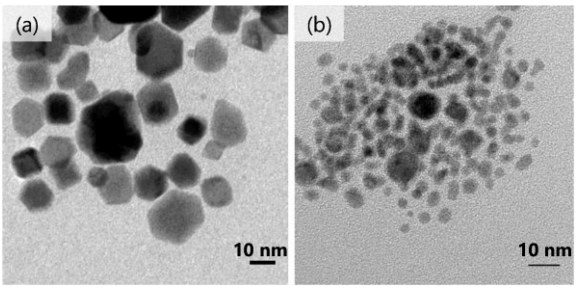

Fig. 7 TEM Images of Pt–NP (a) and SnPt–NP (Sn/Pt = 1.40) (b) Catalysts[24]

Figure 8 shows the XRD patterns of SnPt–NP catalysts with different Sn/Pt ratios. In the cases of Sn/Pt = 0 (Pt–NP) (**Fig. 8** (a)) and 0.48 (**Fig. 8** (b)), the observed peaks were characteristic of fcc Pt and fcc Sn_1Pt_3, respectively. Peaks of Sn_1Pt_3 and Sn_1Pt_1 were observed at Sn/Pt = 0.71 and 0.92 (**Figs. 8** (c) and (d), respectively). In this ratio range, the intensities of the Sn_1Pt_3 and Sn_1Pt_1 peaks decreased and increased, respectively, with higher Sn content. Only Sn_1Pt_1 peaks were observed at Sn/Pt = 1.40 and 1.51 (**Figs. 8** (e) and (f), respectively), and Sn_2Pt_1 peaks were detected at Sn/Pt = 2.19 (**Fig. 8** (g)). Thus, the formation of Sn_xPt_y alloys in SnPt–NP catalysts could be controlled by varying the initial $Pt(acac)_2$: $Sn(OAc)_2$ ratio.

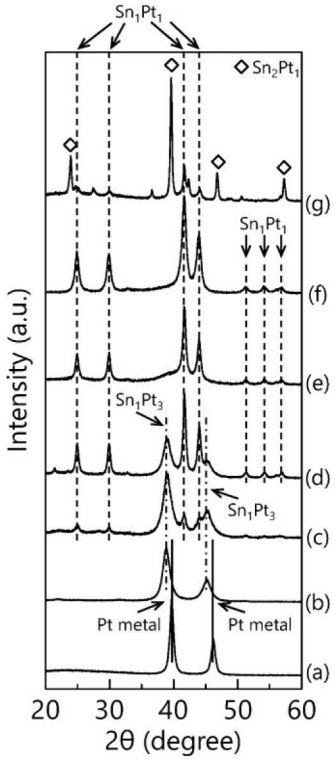

The diffraction patterns were recorded at a scanning speed of 0.5°/min.

Fig. 8 XRD Patterns of SnPt-NP Catalysts Prepared by Polyalcohol Reduction with Sn/Pt = 0 (a), 0.48 (b), 0.71 (c), 0.92 (d), 1.40 (e), 1.51 (f), and 2.19 (g)[24]

3. 3. Relationship between Sn_xPt_y Alloy Composition and Crotonaldehyde Hydrogenation Performance of SnPt-NP Catalysts

To investigate the relationship between Sn_xPt_y alloy structures in SnPt-NP catalysts and catalytic performance, liquid-phase hydrogenation of crotonaldehyde (0.2 mL) in 2-methyl-2-butanol (4.0 mL) was carried out over NP catalysts (10 mg) in a stainless-steel autoclave (30 mL) at 373 K under H_2 at 2.0 MPa (gauge) for 0.5 h (**Fig. 9**). SAL was predominantly produced over Pt-NP (Sn/Pt = 0) (**Fig. 9(b)**). Crotonaldehyde conversion was maximized at Sn/Pt = 0.49, subsequently decreasing with higher Sn content (**Fig. 9(a)**). SAL selectivity decreased with higher Sn/Pt ratio up to 1.40, subsequently increasing at Sn/Pt ≥ 1.51 (**Fig. 9(b)**). The highest SOL selectivity was obtained at Sn/Pt = 0.48 and remained almost constant in the range Sn/Pt = 0.71-2.19 (**Fig. 9(b)**). The maximum UOL selectivity was obtained as 71.5 % at 37.6 % conversion over the SnPt-NP catalyst with Sn/Pt = 1.40 (**Fig. 9(b)**).

Scheme 3 shows the suggested mechanism of crotonaldehyde hydrogenation over SnPt-NP catalysts. At Sn/Pt = 0.48, the formation of Sn_1Pt_3 was confirmed by XRD (**Fig. 8** (b)), and the crotonaldehyde conversion (**Fig. 9(a)**) and UOL and SOL selectivities (**Fig. 9(b)**)

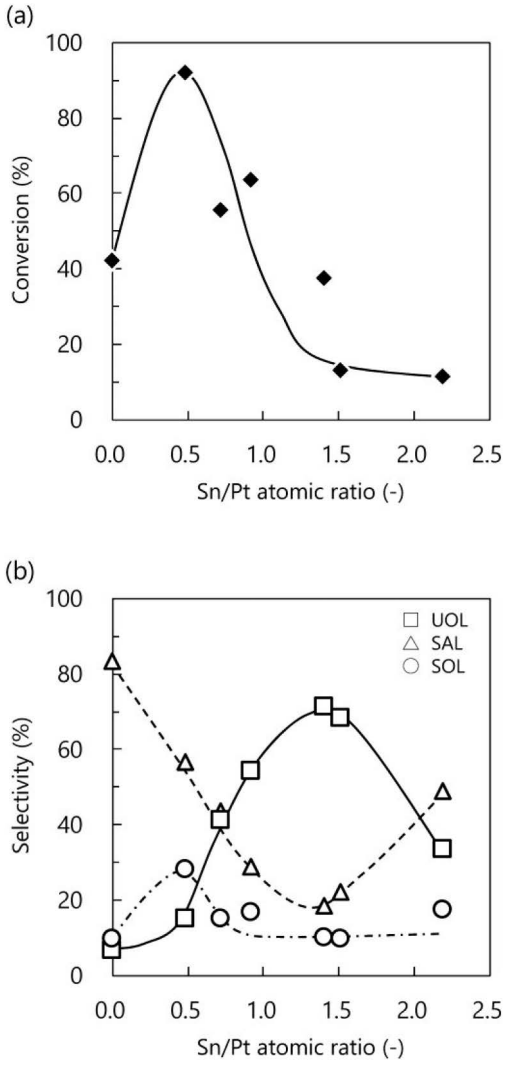

Fig. 9 Effect of the Sn/Pt Atomic Ratio of SnPt-NP Catalysts Prepared by Polyalcohol Reduction on (a) Conversion and (b) Product Formation Selectivity during Crotonaldehyde Hydrogenation[24]

were improved compared with those for Pt-NP catalysts, which suggested that the Sn_1Pt_3 alloy can accelerate not only C = O activation but also H_2 and/or C = C activation. At Sn/Pt = 0.71-1.51, the Sn_1Pt_3 to Sn_1Pt_1 transition proceeded with higher Sn content (**Figs. 8** (c)-(f)). Notably, the catalytic activity decreased (**Fig. 9(a)**), but the UOL selectivity increased with higher Sn content for Sn_1Pt_1 alloy formation (**Fig. 9(b)**). This behavior agrees well with the results obtained for SiO_2-supported SnPt catalysts (**Figs. 1-4**). These results strongly suggest that Sn_1Pt_1 features higher UOL formation selectivity and lower H_2 activation activity than Sn_1Pt_3. As shown in **Fig. 7**, the SnPt-NP catalyst with Sn/Pt = 1.40 contained smaller particles than Pt-NP. The size of metal particles in a catalyst is well known to affect catalytic activity. Cinnamaldehyde conversion increased with smaller particle

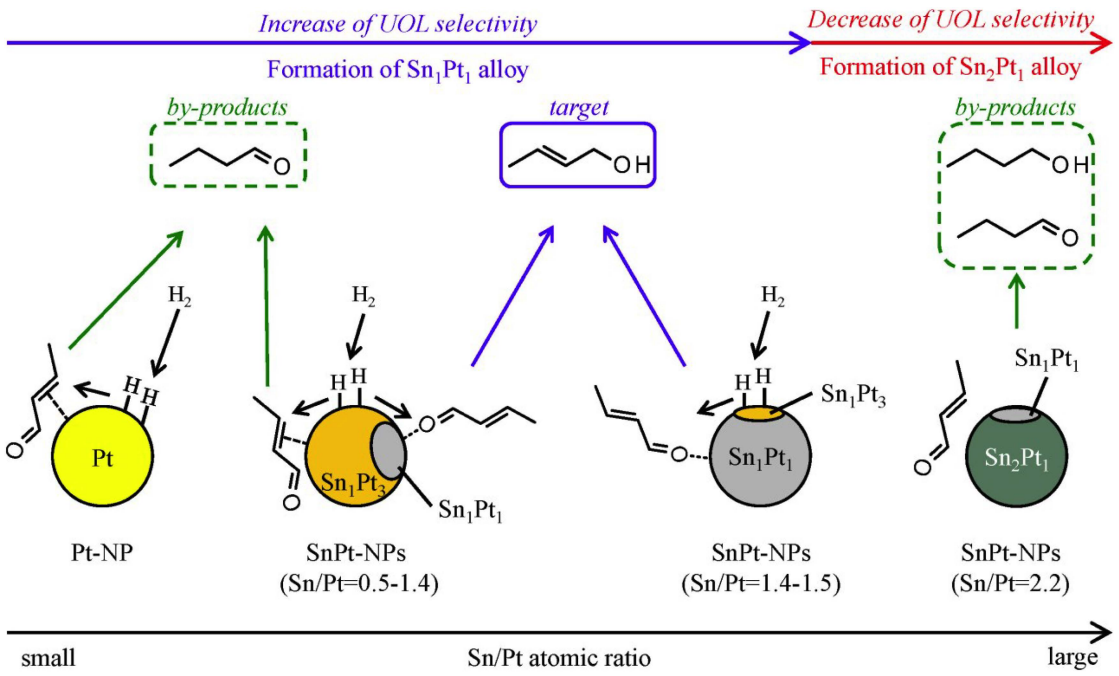

Scheme 3 Suggested Mechanism of Crotonaldehyde Hydrogenation over SnPt–NP Catalysts with Various Sn/Pt Atomic Ratios[24)]

size of Pt nanoparticle catalysts[37)]. Despite the smaller particle diameter, crotonaldehyde conversion over the SnPt–NP catalyst with Sn/Pt = 1.40 was almost the same as that over the Pt–NP catalyst, implying that Sn_1Pt_1 has a lower H_2 activation activity than Sn_1Pt_3. Sn_2Pt_1 alloy is mainly formed in the SnPt–NP catalyst with constant Sn/Pt ratio of 2.19 (**Fig. 8** (g)), and the UOL and SAL selectivities over this alloy are lower and higher, respectively, than those over Sn_1Pt_1 (**Fig. 9(b)**). The formation of Sn_2Pt_1 over Pt/SnO_2 catalysts was reported to decrease UOL selectivity[15)]. As mentioned earlier in Section **2.**, similar behavior was observed for Sn_2Pt_1 on $Sn/Pt/SiO_2$ catalysts (Sn/Pt = 2.0) (**Figs. 3(b)** and **4** (h)). Thus, Sn_2Pt_1 was concluded to be ineffective for UOL formation.

The results of catalytic performance screening for the selective hydrogenation of crotonaldehyde over SnPt–NP catalysts revealed that SnPt (Sn_1Pt_3, Sn_1Pt_1, and Sn_2Pt_1) alloys had higher selectivity for UOL formation than reduced Pt metal. The highest UOL selectivity was obtained for SnPt–NP (Sn/Pt = 1.40) catalysts with a uniform Sn_1Pt_1 alloy structure, which was concluded to be the most effective among the Sn_xPt_y phases for UOL formation during the hydrogenation of unsaturated aldehydes to the corresponding unsaturated alcohols.

The improvement of UOL selectivity during the Pt → Sn_1Pt_3 → Sn_1Pt_1 transition is presumably due to the dilution of Pt ensembles by the added Sn species. A previous diffuse-reflectance infrared Fourier transform spectroscopy study showed that strong crotonaldehyde adsorption through the C = C bond (assigned to the di-σ_{CC} adsorption mode over the Pt surface) was observed over Pt/TiO_2 catalysts reduced with H_2 at 573 K[40)]. The di-σ_{CC} adsorption configuration requires at least two adjacent Pt atoms, forming a Pt ensemble. The number of Pt ensembles decreased with the Pt → Sn_1Pt_3 → Sn_1Pt_1 transition, which suppressed C = C bond hydrogenation. A previous infrared spectroscopy study showed that Sn is important in the enhancement of the donating-on-top adsorption of propionaldehyde on Sn species through the carbonyl group oxygen[41)]. As the carbonyl group of crotonaldehyde can be adsorbed in the donating-on-top η^1(O) configuration on one Sn atom, the increase of Sn content in Sn_xPt_y enhances activation of this group. The dilution of Pt ensembles by metallic Sn not only suppresses C = C bond activation, but also enhances C = O bond activation and thus increases the selectivity for UOL formation over Sn_1Pt_3 and Sn_1Pt_1. The Sn content of Sn_2Pt_1 exceeds that of Sn_1Pt_1, but the UOL selectivity decreased from Sn_1Pt_1 to Sn_2Pt_1, which suggests that at least one lattice plane of Sn_2Pt_1 contains Pt ensemble sites. Therefore, the mechanism of hydrogenation over Sn_2Pt_1 requires further investigation.

4. Conclusion

Selective liquid-phase hydrogenation of crotonaldehyde was investigated over SiO_2-supported SnPt catalysts and unsupported SnPt nanoparticulate catalysts. The relationship between the Sn_xPt_y alloy composition of the obtained catalysts and their activity for crotonaldehyde hydrogenation was also studied, with the key findings summarized below.

(1) The maximum UOL selectivity observed over Sn/Pt/SiO_2 catalysts prepared by successive impregnation exceeded that observed over Sn–Pt/SiO_2 catalysts prepared by co-impregnation. At the same Sn/Pt atomic ratio, the impregnation method affected the formation of Sn_xPt_y alloys, and thus the catalytic performance for selective crotonaldehyde hydrogenation.
(2) Unsupported SnPt–NP catalysts with several types of Sn_xPt_y alloy phases were synthesized by varying the amount of $Sn(OAc)_2$ introduced during the polyalcohol reduction method. SnPt–NP catalysts with Sn/Pt = 0.48 and 1.40 contained uniform Sn_1Pt_3 and Sn_1Pt_1 alloy phases, respectively.
(3) Sn_xPt_y species were suggested to affect the performance of both supported and non-supported SnPt catalysts. Sn_1Pt_3, Sn_1Pt_1, and Sn_2Pt_1 alloys achieved higher UOL formation selectivities than reduced Pt metal. The $Sn_1Pt_3 \rightarrow Sn_1Pt_1$ phase transition increased UOL formation selectivity, whereas Sn_2Pt_1 alloy formation decreased it. Sn_1Pt_1 was suggested to carry the most effective sites for the selective production of unsaturated alcohols from the corresponding aldehydes.

Acknowledgment

We thank Mr. Kenji Nomura and Mr. Norihisa Kumagai, Faculty of Engineering, Kobe University, for assistance with H_2 and CO chemisorption and BAT measurements, and express our gratitude to Professor Shik Chi Edman Tsang of The University of Oxford for support with SnPt–NP catalyst preparation.

References

1) Ponec, V., *Appl. Catal. A: Gen.*, **149**, 27 (1997).
2) Claus, P., *Top. Catal.*, **5**, 51 (1998).
3) Mäki-Arvela, P., Hájek, J., Salmi, T., Muzin, D. Y., *Appl. Catal. A: Gen.*, **292**, 1 (2005).
4) Tamura, M., Nakagawa, Y., Tomishige, K., *J. Jpn. Petrol. Inst.*, **62**, (3), 106 (2019).
5) Marinelli, T. B. L. W., Ponec, V., *J. Catal.*, **156**, 51 (1995).
6) Englisch, M., Ranade, V. S., Lercher, J. A., *J. Mol. Catal. A: Chem.*, **121**, 69 (1997).
7) Coloma, F., Sepúlveda-Escribano, A., Fierro, J. L. G., Rodríguez-Reinoso, F., *Appl. Catal. A: Gen.*, **136**, 231 (1996).
8) Altmann, L., Wang, X., Borchert, H., Kolny-Olesiak, J., Zielasek, V., Parisi, J., Kunz, S., Bäumer, M., *Phys. Chem. Chem. Phys.*, **17**, 28186 (2015).
9) Santori, G. F., Casella, M. L., Siri, G. J., Adúriz, H. R., Ferretti, O. A., *Appl. Catal. A: Gen.*, **197**, 141 (2000).
10) Ruiz-Martínez, J., Coloma, F., Sepúlveda-Escribano, A., Anderson, J. A., Rodríguez-Reinoso, F., *Catal. Today*, **133-135**, 35 (2008).
11) Hou, F., Zhao, H., Song, H., Chou, L., Zhao, J., Yang, J., Yan, L., *RSC Adv.*, **7**, 48649 (2017).
12) Stassi, J. P., Zgolicz, P. D., de Miguel, S. R., Scelza, O. A., *J. Catal.*, **306**, 11 (2013).
13) Coloma, F., Llorca, J., Homs, N., Ramírez de la Piscina, P., Rodríguez-Reinoso, F., Sepúlveda-Escribano, A., *Phys. Chem. Chem. Phys.*, **2**, 3063 (2000).
14) Zgolicz, P. D., Rodríguez, V. I., Vilella, I. M. J., de Miguel, S. R., Scelza, O. A., *Appl. Catal. A: Gen.*, **392**, 208 (2011).
15) Liberková, K., Touroude, R., *J. Mol. Catal. A: Chem.*, **180**, 221 (2002).
16) Santori, G. F., Casella, M. L., Siri, G. J., Adúriz, H. R., Ferretti, O. A., *React. Kinet. Catal. Lett.*, **75**, 225 (2002).
17) Coloma, F., Sepúlveda-Escribano, A., Fierro, J. L. G., Rodríguez-Reinoso, F., *Appl. Catal. A: Gen.*, **148**, 63 (1996).
18) Margitfalvi, J. L., Tompos, A., Kolosova, I., Valyon, J., *J. Catal.*, **174**, 246 (1998).
19) Margitfalvi, J. L., Vankó, G., Borbáth, I., Tompos, A., Vértes, A., *J. Catal.*, **190**, 474 (2000).
20) Taniya, K., Yu, C. H., Tsang, S. C., Ichihashi, Y., Nishiyama, S., *Catal. Commun.*, **14**, 6 (2011).
21) Taniya, K., Jinno, H., Kishida, M., Ichihashi, Y., Nishiyama, S., *J. Catal.*, **288**, 84 (2012).
22) Taniya, K., Hara, T., Imai, T., Ichihashi, Y., Nishiyama, S., *J. Chem. Eng. Jpn.*, **47**, 130 (2014).
23) Durussel, P., Massara, R., Feschotte, P., *J. Alloys Compd.*, **215**, 175 (1994).
24) Taniya, K., Yu, C. H., Takado, H., Hara, T., Okemoto, A., Horie, T., Ichihashi, Y., Tsang, S. C., Nishiyama, S., *Catal. Today*, **303**, 241 (2018).
25) Taniya, K., Ichihashi, Y., Nishiyama, S., *Catal. Catal.*, **55**, 110 (2013).
26) Ito, S., Tomishige, K., *Catal. Commun.*, **12**, 157 (2010).
27) Hori, K., Matsune, H., Takenaka, S., Kishida, M., *Sci. Technol. Adv. Mater.*, **7**, 678 (2006).
28) Kwak, D.-H., Lee, Y.-W., Han, S.-B., Hwang, E.-T., Park, H.-C., Kim, M.-C., Park, K.-W., *J. Power Sources*, **275**, 557 (2015).
29) Llorca, J., Homs, N., Fierro, J.-L. G., Sales, J., Ramírez de la Piscina, P., *J. Catal.*, **166**, 44 (1997).
30) Colmati, F., Antolini, E., Gonzalez, E. R., *J. Solid State Electrochem.*, **12**, 591 (2008).
31) Paál, Z., Wootsch, A., Teschner, D., Lázár, K., Sajó, I. E., Győrffy, N., Weinberg, G., Knop-Gericke, A., Schlögl, R., *Appl. Catal. A: Gen.*, **391**, 377 (2011).
32) Niwa, M., Inagaki, S., Murakami, Y., *J. Phys. Chem.*, **89**, 2550 (1985).
33) Niwa, M., Inagaki, S., Murakami, Y., *J. Phys. Chem.*, **89**, 3869 (1985).
34) Niwa, M., Matsuoka, Y., Murakami, Y., *J. Phys. Chem.*, **91**, 4519 (1987).
35) Taniya, K., Izumi, A., Ichihashi, Y., Nishiyama, S., *Mater. Sci. Forum*, **658**, 420 (2010).
36) Segawa, A., Taniya, K., Ichihashi, Y., Nishiyama, S., Yoshida, N., Okamoto, M., *Ind. Eng. Chem. Res.*, **57**, 70 (2018).
37) Tsang, S. C., Cailuo, N., Oduro, W., Kong, A. T. S., Clifton, L., Yu, K. M. K., Thiebaut, B., Cookson, J., Bishop, P., *ACS Nano*, **2**, 2547 (2008).
38) Oduro, W. O., Cailuo, N., Yu, K. M. K., Yang, H., Tsang, S. C., *Phys. Chem. Chem. Phys.*, **13**, 2590 (2011).
39) Somodi, F., Peng, Z., Getsoian, A. B., Bell, A. T., *J. Phys. Chem. C*, **115**, 19084 (2011).
40) Dandekar, A., Vannice, M. A., *J. Catal.*, **183**, 344 (1999).
41) Nishiyama, S., Hara, T., Tsuruya, S., Masai, M., *J. Phys. Chem. B*, **103**, 4431 (1999).

要　　旨

SnPt 二元系触媒における Sn_xPt_y 合金構造が不飽和アルデヒドの選択水素化に及ぼす影響

谷屋　啓太，市橋　祐一，西山　　覚

神戸大学大学院工学研究科応用化学専攻，657-8501 神戸市灘区六甲台町1-1

不飽和アルデヒドから不飽和アルコールへの選択水素化における触媒性能のさらなる向上には，不均一触媒における活性点構造を深く理解する必要がある。SnPt 二元系触媒では，合金を形成する Sn 金属が選択性に強く影響を及ぼす重要な要因の一つと考えられている。本稿では，Sn/Pt 原子比が異なる担持および非担持の SnPt 二元系触媒上でのクロトンアルデヒドの水素化反応における Sn_xPt_y 合金構造と触媒性能の関係について解説する。SnPt 二元系触媒調製時の Sn/Pt 原子比が同じでも，調製方法の違いにより異なる合金相が形成した。本研究では，Sn_1Pt_3，Sn_1Pt_1，および Sn_2Pt_1 合金の形成を確認し，いずれの合金も Pt 金属より高いクロチルアルコール選択性を示した。共含浸および逐次含浸で調製した担持触媒およびポリアルコール還元法で調製した非担持触媒のいずれにおいても，Sn_1Pt_3 合金構造から Sn_1Pt_1 合金構造に相変化するに従ってクロチルアルコールの選択率が向上した。また，さらに Sn 含有量が多い Sn_2Pt_1 合金構造が触媒上に形成するとクロチルアルコールの選択率が低下した。不飽和アルデヒドの水素化反応において Sn_1Pt_1 合金構造が不飽和アルコールの形成に最も有効な合金構造であった。

……